Supporting information for

Polymer/iron-oxide nanocomposite adsorbents for cycled magnetically-enabled extraction of aqueous micropollutants

Eoin P. McKiernan, Alexa Ennis, Colm Delaney, Larisa Florea, Dermot F. Brougham

B.Sc. E. McKiernan, Prof. D. F. Brougham

School of Chemistry, University College Dublin, Belfield, Dublin 4, Ireland

E-mail: dermot.brougham@ucd.ie

B.Sc. A. Ennis, Ph.D. L Florea

School of Chemistry & AMBER, the SFI Research Centre for Advanced Materials and BioEngineering Research, Trinity College Dublin, the University of Dublin.

1. Nanoflower preparation

Iron oxide nanoflowers were synthesized using a minor adaptation of the procedure developed by Hugounenq *et al.*, [1] producing stable aqueous suspensions of NFs with an average metallic core size of 22.5 ± 2.3 and hydrodynamic size of 35 ± 2.1 nm, with low polydispersity index of 0.124 ± 0.064, see **Figure S1**.

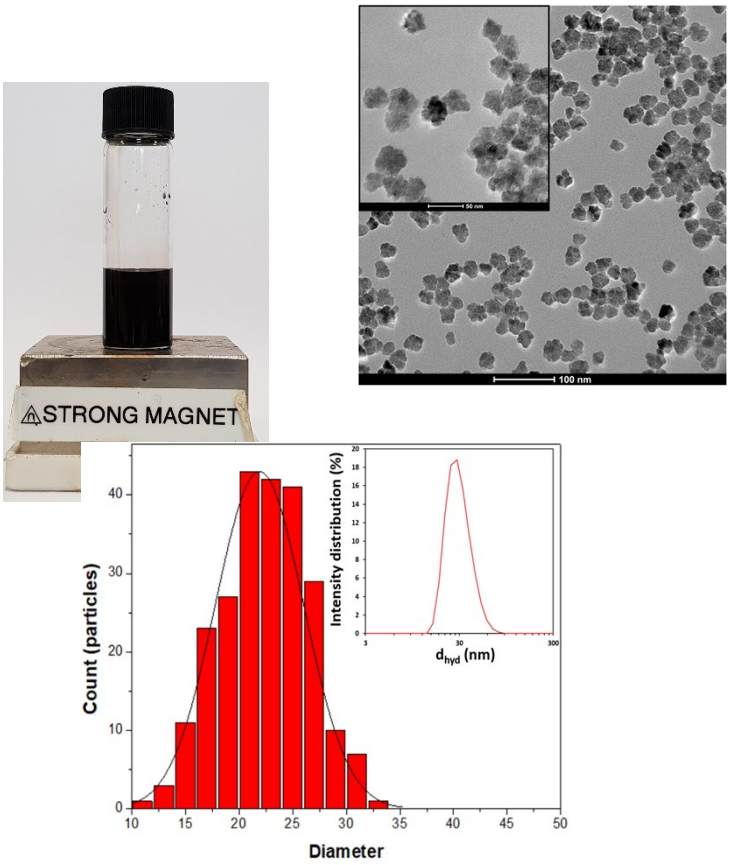

Figure S1. TEM micrograph of IONFs at 80k x magnification, inset at 150k x (left). Particle size distribution analysis of TEM images with inset of intensity size distribution by DLS (right).

2. Polymer nanocomposites

The NF-TET suspension was prepared by addition of concentrated aqueous nanoflower suspension for every mL of TET-BAPO to generate the appropriate concentration. Excellent miscibility ensured the same outcome for all starting formulations. The mixture was then vortexed until the suspension appeared homogeneous. Dynamic light scattering analysis confirms full dispersion of the NFs in neat TET912 macromonomer (viscosity 63 cP, which was used for the DLS analysis), the hydrodynamic size remained relatively unchanged compared to the aqueous disperision (34.8 to 37.3 nm) with monodispersity being retained (PDI: 0.079 to 0.090). This also shows that there is minimal interaction between the macromonomer and the particle surfaces. SEM analysis of the polymerized composite material further illustrates the excellent particle dispersion, with the estimated average interparticle distance of the dispersed NFs being 776 ± 237 nm, which far exceeds the minimim distance required for magnetic dipolar interactions to occur. As a result the effective magnetocrystalline isotropy of each dispersed NF is unnaffected, thus retaining their superparamagnetic properties.

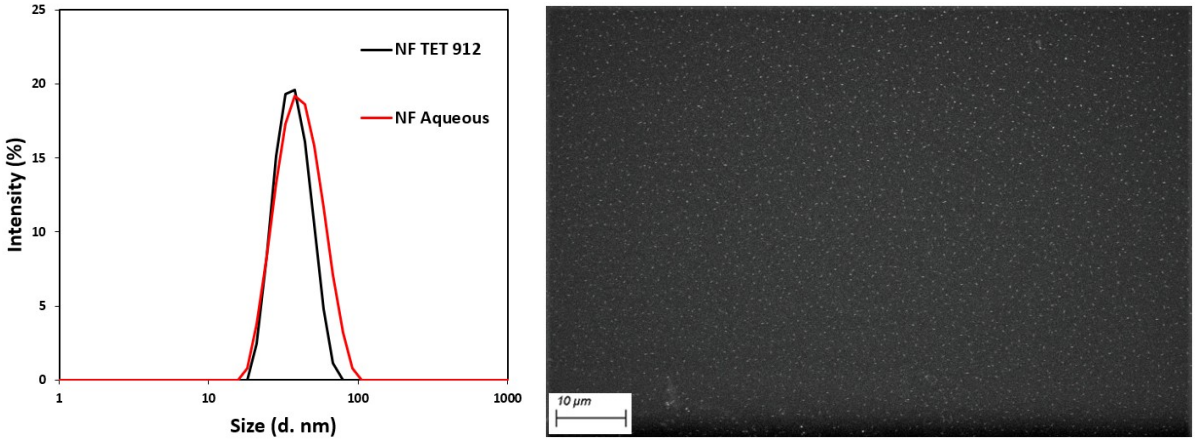

Figure S2. Left: DLS Size distribution by intensity trends for NFs dispersed in water and TET912. Right: SEM micrograph of a cross sections of polymerized NF-TET912.

3. Micropollutants studied

Table S1. Description and literature references of the micropollutants investigated

Compound	Category	Detected concentration in the reported study ($\mu g\ L^{-1}$)	Reference
Ciprofloxacin	Antibiotic	1.27	Mahmood et al. (2019)[2]
Doxorubicin hydrochloride	Chemotherapeutic	0.042	Jureczkoa et al. (2019)[3]
Eriochrome Black T	Complexometric indicator		Moeinpour et al(2014)[4]
Fluorescein	Medical dye		Al-Kadhi et al. (2020)[5]
Malachite Green Oxalate	Textile dye & antimicrobial agent		Wang et al. (2014)[6]

Methylene Blue	Textile dye and blood medication		Fito et al. (2020)[7]
Rhodamine B	Tracer dye	3.14	Soylak et al. (2011)[8]
Salicylic acid	Analgesic	2.18	Evgenidou et al. (2015)[9]

The micropollutants investigated have a variety of molecular properties. This allowed the identification of trends in adsorption performance with regards to the molecular structure of the pollutants, facilitating better understanding of the mechanisms of interaction contributing to adsorption and helping establish criteria for improved adsorbent performance. A summary of the range molecular properties identified in the micropollutants investigated is provided in **Table S2.**

Table S2. Summary of the molecular properties and value ranges of the micropollutants investigated.

Molecular property	**Range**	**Unit**
Aqueous solubility	0.02 - 500	mg mL^{-1}
H Bond acceptors	2 - 9	
H bond donors	0 - 6	
Molecular weight (Da)	138 - 543	Da
π electrons	8 - 28	
Topological polar surface area	6.2 – 206.1	$Å^2$

The properties listed in **Table S2** may impact the adsorption capacity of the analyte value for a number of reasons. The aqueous solubility of a molecule may influence adsorption capacity as the adsorption process is in competition with the solvation interactions the molecule is experiencing with the dispersion solvent. The presence of hydrogen bond donors may facilitate hydrogen bonding with the oxygen atoms in the ethoxylate chains in TET. Molecules with high molecular weight may occupy more adsorption sites or have more limited diffusion driven penetration into the adsorbent as compared to low MW molecules. Finally, the number of π electrons in the structure may facilitate attractive n – π interactions. NF-TET discs were submerged in 100 $mg.L^{-1}$ aqueous stock solutions of the 8 micropollutants for 24 h at which point no further adsorption was observed in all cases.

4. Micropollutants spectroscopic data

The molecular structure, UV-Vis spectra, linear UV-Vis range and adsorption capacity of each micropollutant are presented in **Figure S3**.

Ciprofloxacin

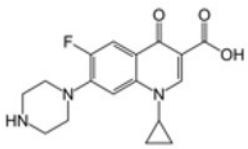

q = 0.53 mg g^{-1}

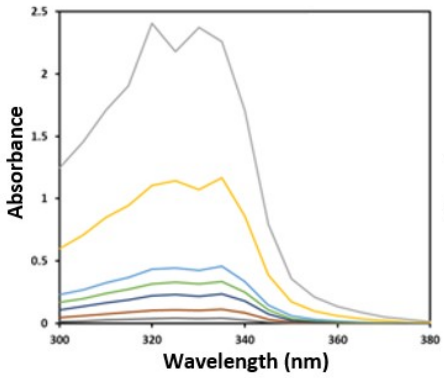

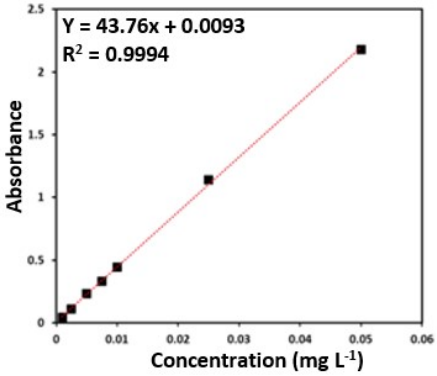

Doxorubicin

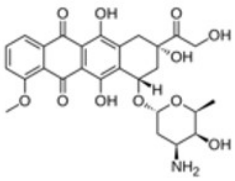

q = 0.67 mg g^{-1}

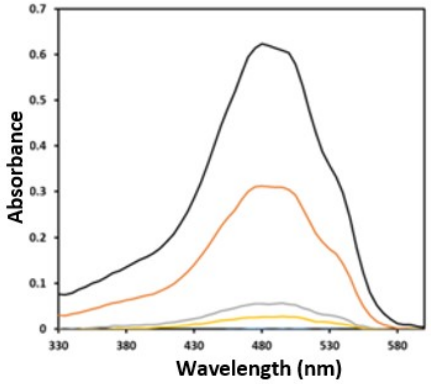

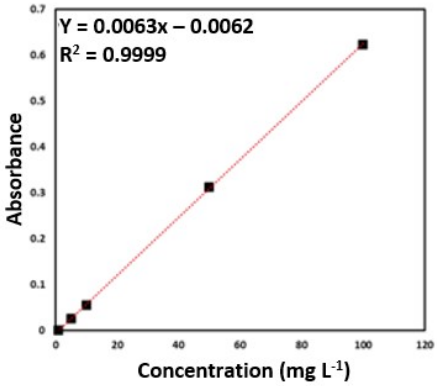

Eriochrome Black T

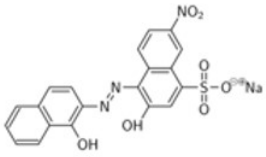

q = 1.2 mg g^{-1}

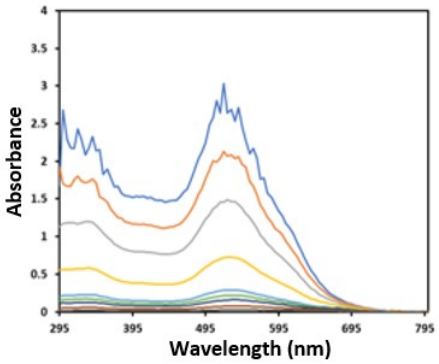

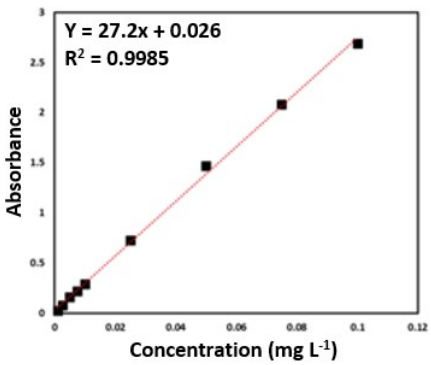

Fluorescein

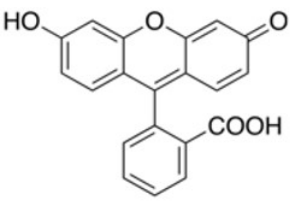

q = 1.4 mg g^{-1}

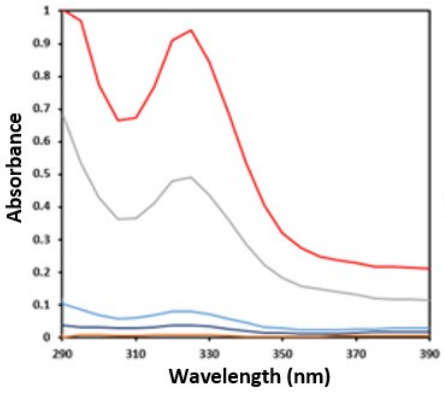

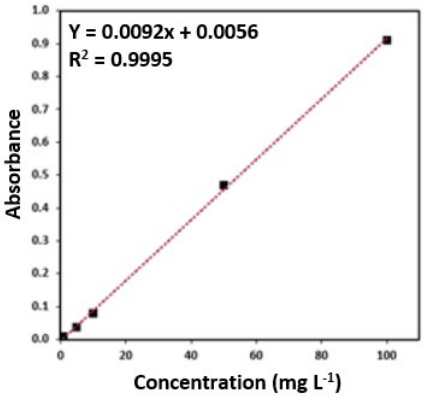

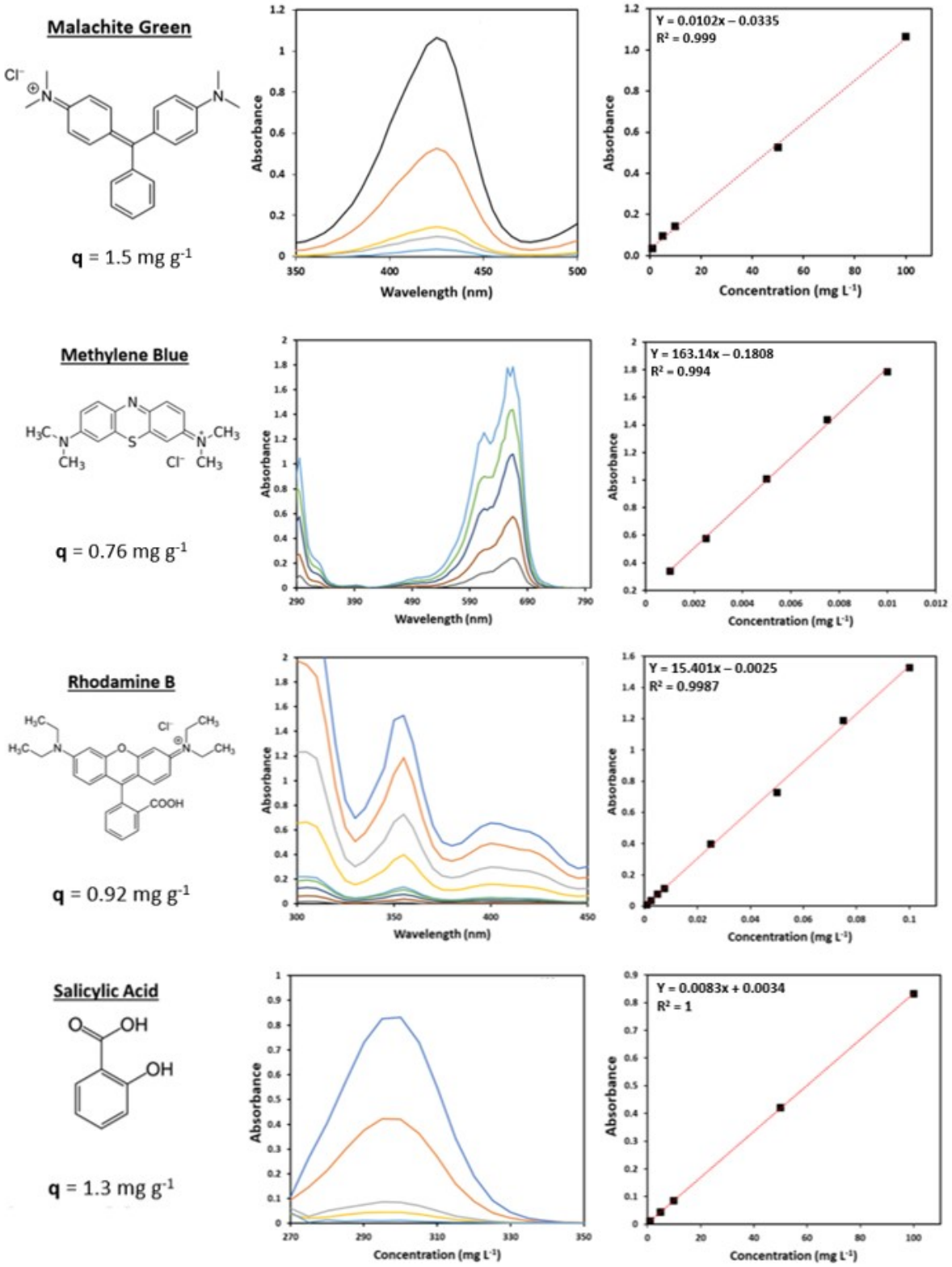

Figure S3. Molecular structures, adsorption capacity, UV-Vis spectrum and linear calibration range of the micropollutants.

Table S2. Data extracted from UV-analysis (**Figure S3**) of the micropollutants.

Reagent	**q (mg.g^{-1})**
Ciprofloxacin	0.53
Doxorubicin	0.67
Eriochrome Black T	1.20
Fluorescein	1.40
Malachite Green Oxalate	1.51
Methylene Blue	0.76
Rhodamine B	0.92
Salicylic acid	1.33

5. Adsorption data for NF-TET912 discs

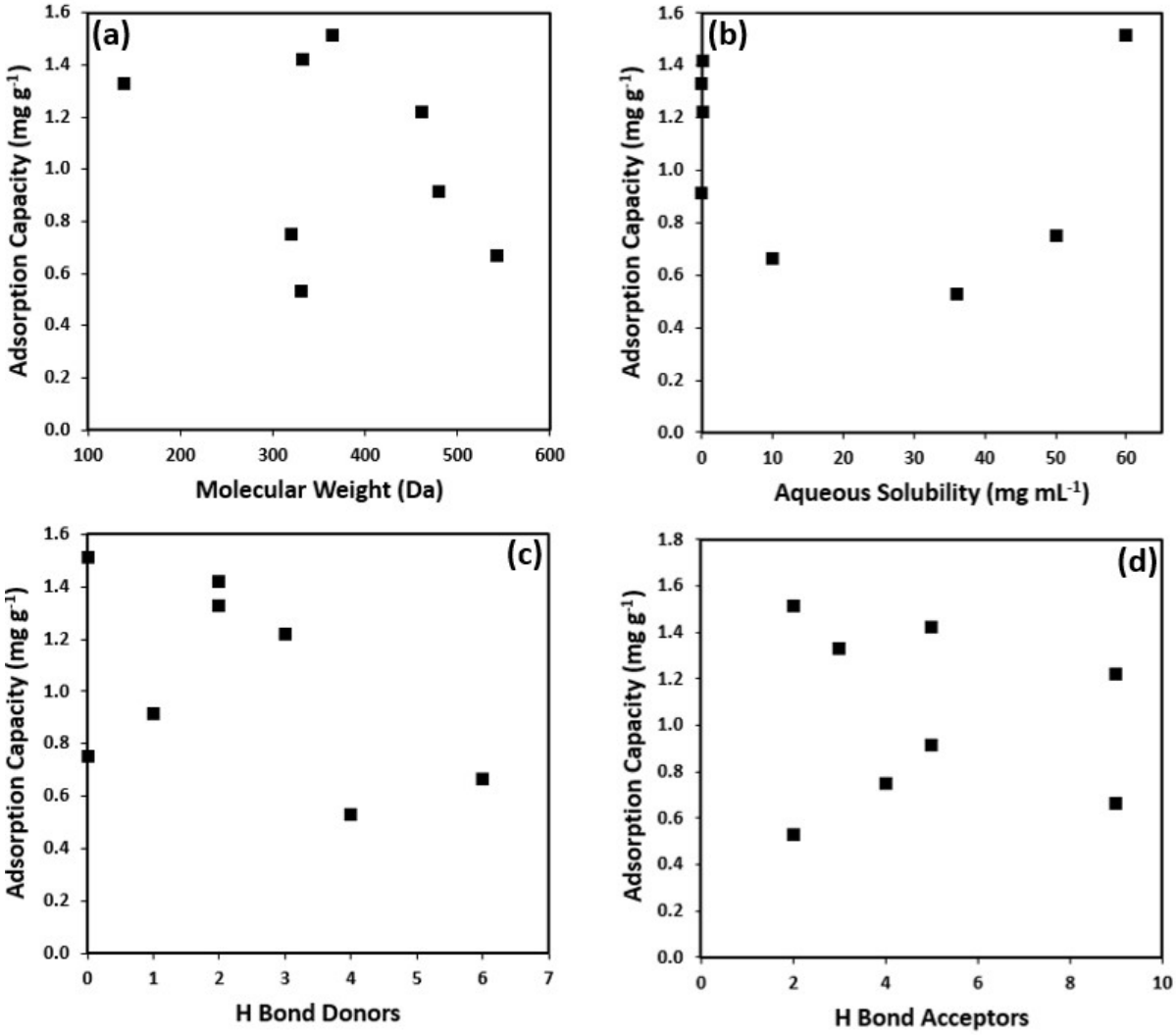

Figure S4. Adsorption capacity of NF-TET912 discs for micropollutants plotted against: (a) Molecular weight, (b) Aqueous solubility, and the number of H-bond donors (c), and acceptors (d).

SI References:

1. P. Hugounenq, M. Levy, D. Alloyeau, L. Lartigue, E. Dubois, V. Cabuil, C. Ricolleau, S. Roux, C. Wilhelm, F. Gazeau, R. Bazzi, *J. Phys. Chem. C.*, 2012, **116**, 15702–15712. L. Lartigue, P. Hugounenq, D. Alloyeau, S. P. Clarke, M. Lévy, J. C. Bacri, R. Bazzi, D. F. Brougham, C. Wilhelm, F. Gazeau, *ACS Nano*, 2012, **6**, 10935–10949.

2. R. Mahmood, H. H. Al-Haideri , F. M. Hassan, *Advances in Public Health*, 2019, 851354.

3. M. Jureczko, J. Kalka, *Eur. J. Pharmacol*. 2020, 866.

4. F. Moeinpour, A. Alimoradi, M. Kazemi, *J. Environ. Heal. Sci. Eng.*, 2014, 12, 1–7.

5. N. S. Al-Kadhi, Int. J. Anal. Chem. 2020, 824368.

6. H. Wang, X. Yuan, G. Zeng, L. Leng, X. Peng, K. Liao, L. Peng, Z. Xiao, *Environ. Sci. Pollut. Res.*, 2014, **21**, 11552–11564.

7. J. Fito, S. Abrham,. K. Angassa, , *Int. J. Environ. Res.*, 2020, **14**, 501–511.

8. M. Soylak, Y. E. Unsal, E Yilmaz, M. Tuzen, *Food Chem. Toxicol.*, 2011, **49**, 1796–1799.

9. I. Pavlakos, T. Arif, A. E. Aliev, W. B. Motherwell, G. J. Tizzard, S. J. Coles. *Angew. Chem. Int. Ed.*, 2015, **54**, 8169 –8174.